SWECLIM
SWEDISH REGIONAL CLIMATE MODELLING PROGRAMME

SMHI

No 99, 2002

Reports Meteorology and Climatology

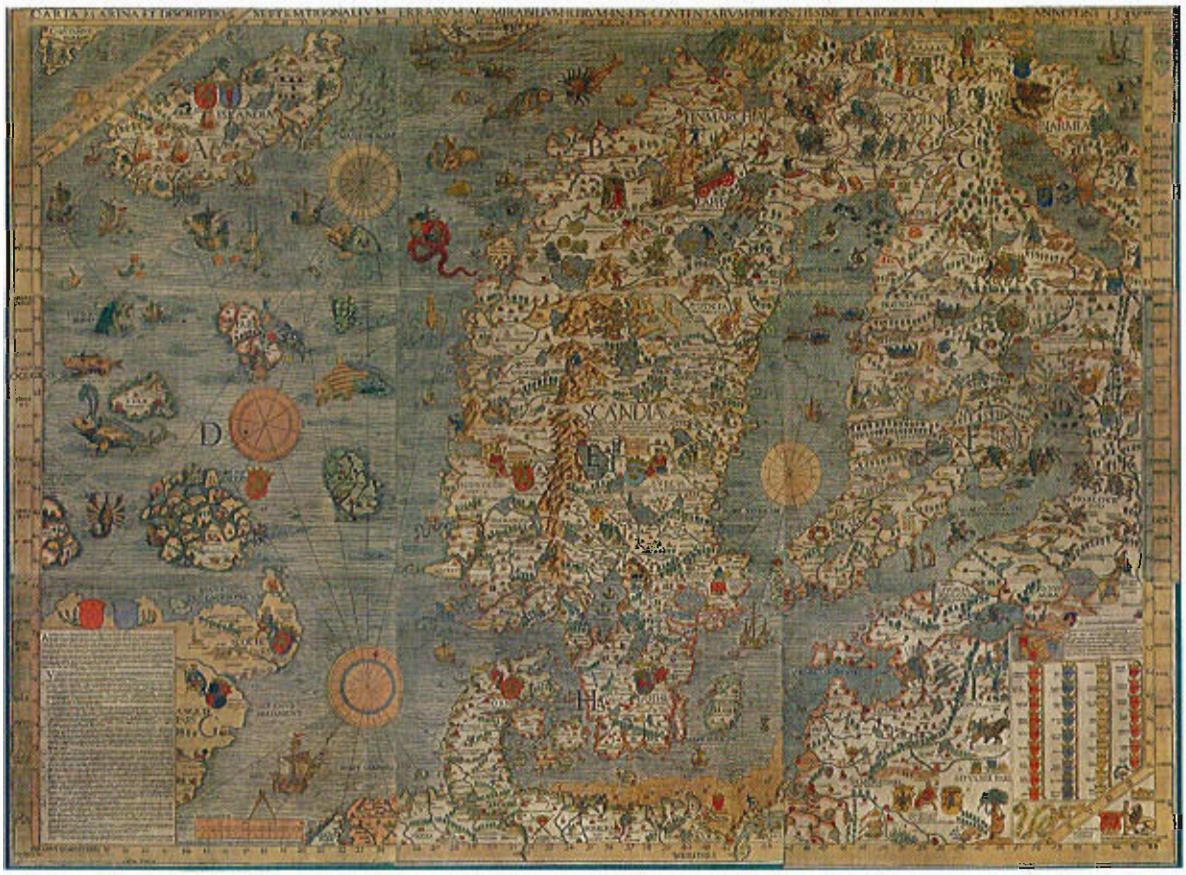

Reconstructing atmospheric surface data for the period 1902-1998 to force a coupled ocean-sea ice model of the Baltic Sea

Frank Kauker
Alfred Wegener Institute for Polar and Marine Research, Germany
H.E. Markus Meier
Swedish Meteorological and Hydrological Institute,
Rossby Centre, Sweden

Cover illustration:

Carta Marina (1539), map of Scandinavia from Olaus Magnus (1490-1557). It was the first large-scale map of any European region. The James Ford Bell Library, University of Minnesota, is acknowledged for making a digital copy of the map available.

RMK
No 99, 2002

Reconstructing atmospheric surface data for the period 1902-1998 to force a coupled ocean-sea ice model of the Baltic Sea

Frank Kauker
Alfred Wegener Institute for Polar and Marine Research, Germany
H.E. Markus Meier
Swedish Meteorological and Hydrological Institute,
Rossby Centre, Sweden

Report Summary / Rapportsammanfattning

Issuing Agency/Utgivare	Report number/Publikation
Swedish Meteorological and Hydrological Institute S-601 76 NORRKÖPING Sweden	RMK No. 99
	Report date/Utgivningsdatum January 2002

Author (s)/Författare

Frank Kauker and H.E.Markus Meier

Title (and Subtitle/Titel

Reconstructing atmospheric surface data for the period 1902-1998 to force a coupled ocean-sea ice model of the Baltic Sea.

Abstract/Sammandrag

A statistical model is developed to reconstruct atmospheric surface data for the period 1902-1998 to force a coupled ocean-sea ice model of the Baltic Sea. As the longest time scale of the Baltic Sea is on the order of 30 years, climate relevant model studies should cover century long simulations. One of the aims of the Swedish Regional Climate Modeling Program is to investigate causes of long-term changes of the Baltic Sea during the past 100 years. However, an observational atmospheric dataset for such a purpose is not available yet. High resolution in space and time is required. Therefore, we developed a statistical model using a *Redundancy Analysis* to reconstruct daily sea level pressure and monthly surface air and dew-point temperature, precipitation, and cloud cover fields on a 1° x 1° regular horizontal grid for the Baltic Sea region. A gridded atmospheric data set based on synoptic stations, which is available for the period 1970-2001, is used as input to the statistical model. Spatial patterns are selected by maximizing predictand variance during the "learning" period 1980-1998. The remainder period 1970-1979 is used for validation. It is shown that the statistical model works reasonable well for all variables. We found the highest skill for sea level pressure and the lowest skill for cloud cover.

Key words/sök-, nyckelord

Baltic Sea, decadal variability, salt water inflows, data reconstruction, atmospheric surface fields, redundancy analysis

Supplementary notes/Tillägg	Number of pages/Antal sidor	Language/Språk
This work is part of the SWECLIM program.	30	English

ISSN and title/ISSN och titel

0347-2116 SMHI Reports Meteorology Climatology

Report available from/Rapporten kan köpas från:

SMHI
S-601 76 NORRKÖPING
Sweden

1 Introduction

The Baltic Sea is one of the world's largest brackish water sea areas with a total surface, excluding the Danish Straits, of 377,400 km^2 and a corresponding volume of 21,200 km^3 (Sjöberg, 1992). The mean water depth amounts to 56 m and the maximum depth to 451 m at Landsort Deep. The highly variable bottom topography separates the water masses into various basins, delimited by high sills or bays (Fig.1). These are, listed from North to South, Bothnian Bay, Bothnian Sea, Åland Sea, Archipelago Sea, Gulf of Finland, Gulf of Riga, Northwestern and Eastern Gotland Basin, Bornholm Basin and Arkona Basin Important channels or sills of the inner Baltic are the Quark separating Bothnian Bay and Bothnian Sea (sill depth of 25 m), the Southern Quark separating Bothnian Sea and Åland Sea (100 m), Stolpe or Slupsk Channel separating Gotland and Bornholm Basin (sill depth of 60 m) and Bornholm Channel separating Bornholm and Arkona Basin (40 m).

The water exchange between the Baltic Sea and the North Sea is restricted by the narrows and sills of the Danish Straits. The width of the narrowest part of the Sound, near Helsingør-Helsingborg, amounts to approximately 4 km. The Sound has a sill depth of only 8 m at its southern entrance at Drogden. Darss Sill, having a depth of about 18 m, separates the Belt Sea from the Arkona Basin.

The mean annual river discharge to the Baltic Sea was 15,310 m^3 s^{-1} for the period 1950-1990 (Bergström and Carlsson, 1994). This inflow originates from a huge drainage basin with a size of 1,729,000 km^2. The river flow is highly variable through the year and there are large inter-annual variations. The lowest (11,132 m^3 s^{-1} in 1976) and highest (18,660 m^3 s^{-1} in 1981) annual values during 1950-1990 differ from the mean value by -27% and $+22\%$, respectively. The maximum recorded monthly average contribution was 32,411 m^3 s^{-1} in May 1966, and the lowest was 7,635 m^3 s^{-1} in December 1959. Less important but not negligible are surface freshwater fluxes (i.e., precipitation minus evaporation). For the period 1981-1994, Omstedt et al. (1997) calculated the total mean atmospheric freshwater inflow to be 1,986 m^3 s^{-1}.

The restricted water exchange through the Danish Straits and the river runoff into the Baltic Sea determine the stratification of the water masses into a homogeneous upper layer and a stratified lower layer. In the pioneering work of Knudsen (1899, 1900), the steady state water exchange was described as a two-layer flow with an outflow in the upper layer and inflow in the lower layer. Transient states of this two-layer fjord-type estuary, in cases of small perturbations, are discussed by Welander (1974).

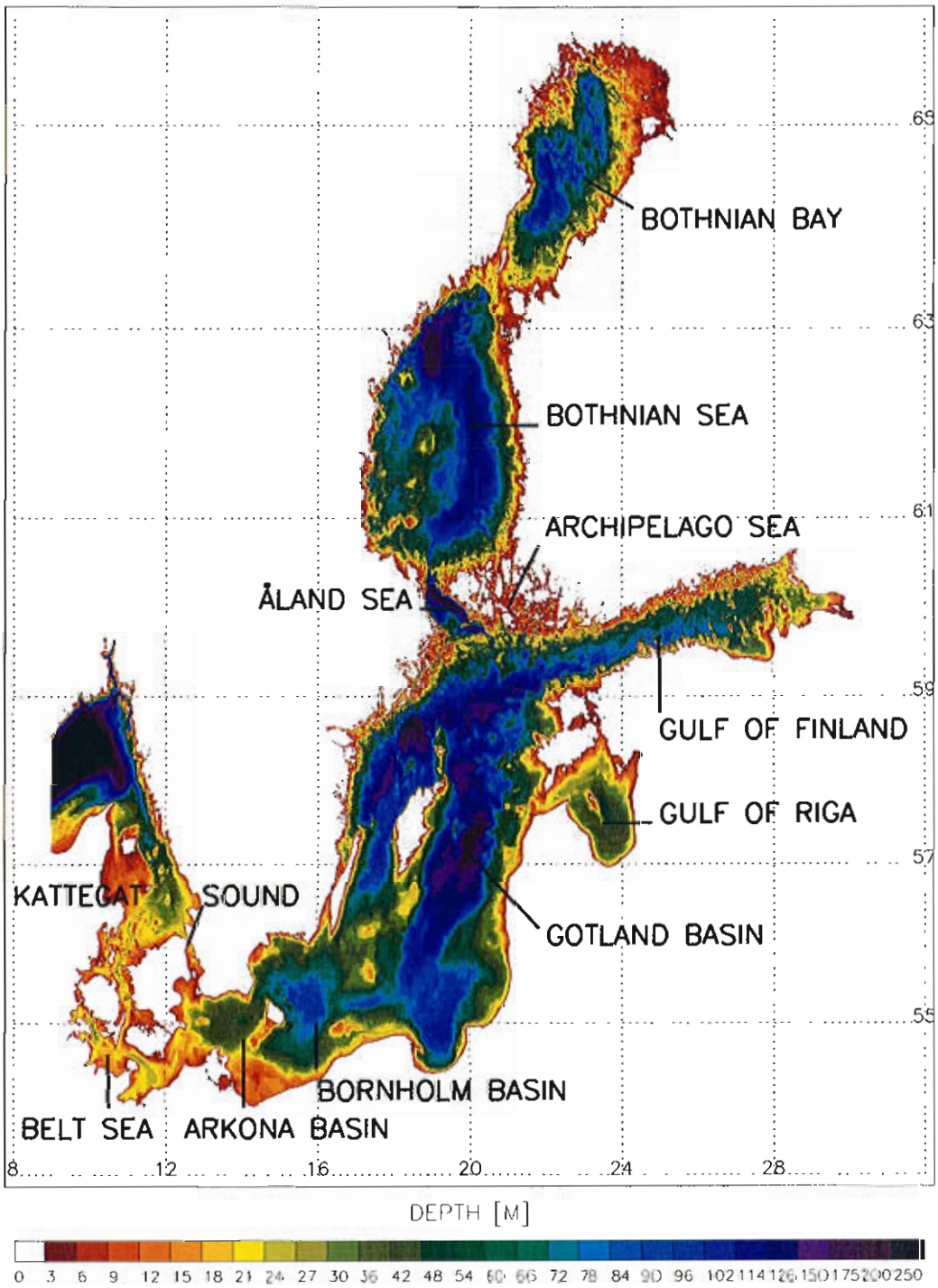

Figure 1: *Bottom topography of the Baltic Sea including Kattegat and Skagerrak (data from Seifert and Kayser, 1995).*

For the past 100 years, Baltic Sea stratification and ventilation of the bottom water in deep sub-basins are affected mainly by large perturbations, so-called major Baltic salt water inflows (Matthäus and Franck, 1992). These events occur randomly during the winter season at intervals of one to several years. They are most probable between November to January, but they occur also in autumn and spring. Major salt water inflows are very likely to be forced by a sequence of easterly winds lasting for 20-30 days followed by strong to very strong westerly winds of similar duration (Lass and Matthäus, 1996). Matthäus and Schinke (1994) discussed mean large scale atmospheric circulation patterns associated with major Baltic inflows between 1899 and 1976. About two weeks before the start of the main inflow period, the Azores High shifts to north-east and its pressure increases. At the same time, the center of lowest pressure moves eastward from the Greenland-Icelandic area to northern Norway, strengthening as it moves. Due to these movements, very strong pressure gradients occur over the North Sea and the entrance area to the Baltic Sea. Matthäus and Schinke (1994) found the maximum gradients occurring two days before and on the first day of the main inflow event.

Since the mid-1970's, the frequency and intensity of major inflows has decreased. They were completely absent between February 1983 and January 1993. During this phase a significant depletion of salt and oxygen occurred, and an increase of hydrogen sulphide were observed in the deep layer of the Gotland Basin. A major salt water inflow in January 1993 terminated this exceptionally long stagnation period (Matthäus and Lass, 1995).

The mechanisms for the decreased frequency of major inflows are discussed in the literature. Lass and Matthäus (1996) argued that the lack of major inflows was due to changes in the wind field over the North Sea and the Baltic Sea. Recently, Schinke and Matthäus (1998) and Matthäus and Schinke (1999) found that variations in river runoff have a greater impact on the occurrence of major inflows than hitherto supposed. They concluded that increased zonal circulation might result in intensified precipitation in the Baltic region and increased river runoff. In addition, river regulation redistributes runoff over many months and gives rise to higher values during autumn and winter. Increased winter runoff (from September to March) seems to reduce the probability of major Baltic inflows. It is also noteworthy that the decreased frequency of major inflows coincides with changes in large scale circulation patterns, i.e., an eastward shift in the position of the North Atlantic Oscillation (NAO) centers of inter-annual variability during the two last decades (Hilmer and Jung, 2000). However, the mechanisms of salt water inflow variability are so far poorly understood.

One of the aims of the Swedish Regional Climate Modeling Program (SWECLIM) is to simulate long-term changes and natural variability of the Baltic Sea (see Meier, 1999; Meier et al., 1999; Meier, 2000; Meier, 2001a, b; Haapala et al., 2001; Meier, 2002a, b; Meier and Faxén, 2002; Meier et al., 2002). The large variability of the forcing functions has already been mentioned. The longest time scale of the system is on the order of 30 years. Thus, to understand the mechanisms of the present Baltic Sea climate, it is necessary to integrate a coupled ice-ocean model for at least 100 years using realistic atmospheric forcing, river runoff and sea level data in the Kattegat. Performing sensitivity experiments it is aimed to answer the important question, why the frequency and intensity of saltwater inflows during the past two decades have decreased. However, whereas long records of river runoff and sea level data in the Kattegat are available, a realistic data set of atmospheric surface fields applicable to force a coupled ice-ocean model of the Baltic Sea is missing. This report describes a method employed for reconstructing such atmospheric surface fields. The focus of the reconstruction is on the ability to simulate major Baltic inflows of high saline water.

Three data sets with century long time-series are available: the sea level pressure station data of Alexandersson et al. (2000), the land and sea temperature fields of Jones (1994), and the land surface precipitation data of Hulme (1992, 1994, 1998).

For the period 1970-2001, a gridded atmospheric data set has been developed at the Swedish Meteorological and Hydrological Institute (SMHI) based on three hourly observations of sea level pressure (SLP), 2 m air temperature, 2 m relative humidity, and total cloud cover. In addition, at 06 and 18 UTC also 12 hourly accumulated precipitation is used. These observations cover the period 1979-2001 only. Data from all available synoptic stations (about 700 to 800) covering the whole Baltic Sea drainage basin are interpolated on a $1^\circ \times 1^\circ$ regular horizontal grid. Thereby, a two-dimensional univariate optimum interpolation scheme is utilized.

The time scales of the long records are analyzed to identify time scales of maximal covariance between the predictor fields and the predictands. The predictand fields for the period 1902-1998 are SLP, surface atmosphere temperature (SAT), dew-point temperature, cloudiness, and precipitation on a $1^\circ \times 1^\circ$ grid for the latitude range $50^\circ N$ to $70^\circ N$ and for the longitude range $8^\circ E$ to $38^\circ E$. The reconstruction of the sea level pressure is based on daily mean data. All other variables enter the calculation as monthly mean values. From the reconstructed SLP geostrophic wind fields are calculated to force the Baltic Sea

model utilizing a boundary layer parameterization to calculate wind speeds in 10 m height (Bumke et al., 1998). It has been shown earlier that applying such wind fields result in realistic mixing conditions (Meier, 2001b) and in realistic sea level variability and sea level means (Meier et al., 2002).

2 Data handling

21 SLP stations are available (Alexandersson et al., 2000) with three values per day, normally recorded at 06, 12, and 18 UTC. For some stations the recorded times shifted from 07, 13, and 20 UTC to the previous mentioned times. Daily means are calculated for the three values per day. If there are missing values, the remaining data are used for the calculation of the daily mean. We are aware that the construction of daily mean values reduces the day-to-day variability, but for the application in mind, the variability for time scales longer than a day is more important than the day-to-day variability. 3 of the 21 stations are skipped because there are too many missing values during the selected time period 1902-1998. The criterion to sort out a station is that there are not more than 200 missing values within one season. We defined the winter season from November to January (and the other seasons correspondingly) because most of the major Baltic inflow events occur during this time. At stations with less than 200 missing values, missing values are replaced by the long term monthly mean daily value. The selected stations are Stykkisholmur (Iceland), Valentia (Ireland), Torshavn (Faeroer Islands), Aberdeen (Great Britain), Bergen (Norway), de Bilt (Netherlands), Oksöy (Norway), Vestervig (Denmark), Nordby (Denmark), Bodö (Norway), Göteborg (Sweden), Lund (Sweden), Härnösand (Sweden), Stockholm (Sweden), Haparanda (Sweden), Visby (Sweden), Kajaani (Finland), and Helsingfors (Finland). Here, the stations are roughly ordered from west to east, which is also the way they are displayed in following plots.

Whereas the SLP data are employed on the daily time scales, the second and third predictor fields are only available as monthly mean values. The SAT anomalies of Jones (1994) are available between 1856 and 1998 on a $5° \times 5°$ grid-box basis. A grid box is considered, if there are less than 50 missing values between 1902 and 1998. Missing values are replaced by the long term monthly mean value. Data are used from the latitude range $40°N$ to $70°N$ and from the longitude range $10°W$ to $40°E$.

The monthly precipitation data from Hulme (1992) cover only land areas between 1900 and 1998 with a resolution of 2.5° in latitude and 3.75° in longitude.

A grid box is considered, if there are less than 80 missing values between 1902 and 1998. Missing values are replaced by the long term mean value. Data are used from the latitude range $45°N$ to $70°N$ and from the longitude range $10°W$ to $40°E$.

The years 1980 to 1998 are selected to be the "learning" period of the statistical model. The period 1970 to 1979 is not taken into account for the building of the model to allow a validation. As already mentioned, the sea level pressure data are reconstructed with the help of daily data. The reconstruction is performed for every season separately to allow for different prediction patterns in each season. All other predictands are reconstructed with monthly data. Here, no separation of the seasons has been performed because of the limited degrees of freedom.

3 Statistical model

A statistical model is used based on a *Redundancy Analysis* (Tyler, 1982; von Storch and Zwiers, 1999).

3.1 Redundancy Analysis

The optimization of the link between the predictor and the predictand is nonsymmetric because the objective is to maximize the variance of the predictand that can be represented. Properties of the predictor patterns, such as the amount of variance they represent, are irrelevant to the problem. The redundancy analysis technique directly addresses this problem by identifying patterns that are strongly linked through a regression model. Patterns are selected by maximizing predictand variance. This technique was developed in the early 1970s by Tyler [1982].

The dimension of the predictor $\vec{X}$ is m_X and the dimension of the predictand $\vec{Y}$ is m_Y. Let us assume that there is a linear operator represented by a $m_X \times k$ matrix Q_k [1]. The regression model that relates $Q_k^T \vec{X}$ is given by

$$\vec{Y} = R(Q_k^T \vec{X}) + \epsilon, \tag{1}$$

[1]The number of columns (patterns) k in Q_k is normally much smaller than the dimension of $\vec{X}$. Thus, the phase space of $\vec{X}$ is reduced by the operator Q_k^T, i.e. only a few patterns are taken into account for the regression.

where R is the $m_Y \times k$ matrix of regression coefficients. The variance represented by $(Q_k^T \vec{X})$ is maximized if $R = \Sigma_{Y,QX}(\Sigma_{QX,QX})^{-1}$, where $\Sigma_{Y,QX} = Cov(\vec{Y}, Q_k^T \vec{X}) = \Sigma_{Y,X} Q_k$ and $\Sigma_{QX,QX} = Q_k^T \Sigma_{XX} Q_k$. Tyler called the proportion of variance, represented by the regression, the *redundancy index* and labeled it

$$R^2(\vec{Y} : Q_k^T \vec{X}) = \frac{tr(Cov(\vec{Y}, \vec{Y}) - Cov(\vec{Y} - \widehat{\vec{Y}}, \vec{Y} - \widehat{\vec{Y}}))}{tr(Cov(\vec{Y}, \vec{Y}))} \tag{2}$$

where $\widehat{\vec{Y}}$ is the estimated value of $\vec{Y}$. $R^2(\vec{Y} : Q_k^T \vec{X})$ is a measure how *redundant* the information in $\vec{Y}$ is, if only the information provided by $\vec{X}$ is known. The redundancy index is invariant to orthogonal transformations of $\vec{Y}$: if A is orthogonal, then $R^2(A\vec{Y} : Q_k^T \vec{X}) = R^2(\vec{Y} : Q_k^T \vec{X})$, i.e. the index does not depend on the basis of $\vec{Y}$. Any squared non-singular matrix Q_{m_X} to transform $\vec{X}$ has also no effect on the redundancy index: $R^2(\vec{Y} : Q_{m_X}^T \vec{X}) = R^2(\vec{Y} : \vec{X})$. However, if Q_k maps $\vec{X}$ onto a k-dimensional subspace $R^2(\vec{Y} : Q_k^T \vec{X}) \leq R^2(\vec{Y} : \vec{X})$. The task is to identify a matrix B which maximizes R^2. Tyler showed that there exists a orthogonal transformation A and a non-singular transformation B such that

$$Cov(B^T \vec{X}, B^T \vec{X}) = I \tag{3}$$

$$Cov(A^T \vec{Y}, B^T \vec{X}) = D \tag{4}$$

where D is a diagonal $m_Y \times m_X$ matrix with elements $d_{jj} = \sqrt{\lambda_i}$ for $j \leq min(m_X, m_Y)$. Further, Tyler showed that the redundancy index $R^2(\vec{Y} : Q_k^T \vec{X})$ is maximized by setting $Q_k = B_k$, where B_k is the $m_X \times k$ matrix that contains the k eigenvectors that correspond to the k largest eigenvalues. Equ. 3 and 4 can be rewritten in the form

$$\Sigma_{YX} \Sigma_{XX}^{-1} \Sigma_{XY} \vec{a}_j = \lambda_j \vec{a}_j \tag{5}$$

$$\Sigma_{XX}^{-1} \Sigma_{XY} \Sigma_{YX} \vec{b}_j = \lambda_j \vec{b}_j. \tag{6}$$

$\vec{X}$ can be expanded in the usual manner

$$\vec{X} = \sum_{j=1}^{m_X} (\vec{X}^T \vec{b}_j) \vec{p}_j, \tag{7}$$

where the adjoint patterns $P = (\vec{p}_1 | \ldots | \vec{p}_{m_X})$ are given by $P^T = B^{-1}$. The part $\widehat{\vec{Y}}$ of $\vec{Y}$ that can be represented by $\vec{X}$ can be expanded as

$$\widehat{\vec{Y}} = \sum_{j=1}^{k} (\widehat{\vec{Y}}^T \vec{a}_j) \vec{a}_j \tag{8}$$

(Note that A is self-adjoint because A is orthogonal.). The expansion coefficient for $\widehat{\vec{Y}}$ can be rewritten

$$\widehat{\vec{Y}}^T \vec{a}_j = \sqrt{\lambda_j} \vec{X}^T \vec{b}_j. \tag{9}$$

It is convenient to apply an empirical orthogonal function (EOF) analysis prior to the redundancy analysis. Then, Σ_{XX} and Σ_{YY} are identity matrices and the computational effort is reduced considerably. A disadvantage is that the predictor variance is reintroduced implicitly.

3.2 Reconstructing the data

$\vec{p}_j$ are the patterns of the predictor $\vec{X}$ which describe maximal variance of the predictand $\vec{Y}$. The predictand is reconstructed with the help of equ. 9. The reconstruction reads

$$\vec{Y}_{rec} = \sum_{j=1}^{k} \sqrt{\lambda_j} (\vec{X}^T \vec{b}_j) \vec{a}_j. \tag{10}$$

For example, if $\vec{X}$ is given for 100 years, equ. 10 allows us to reconstruct $\vec{Y}$ for 100 years.

4 Reconstruction

4.1 Sea Level pressure

The method is demonstrated for winter (November-January). Before describing the predictand and predictor patterns the corresponding time series are depicted in Figure 2 for the first five leading modes. The correlation coefficients between the predictor and predictand time series for the "learning" period are 0.995, 0.971, 0.814, 0.371, 0.050. The black line shows the projection $\vec{X}^T b_j$ for the period 11/1902 to 1/1998 and the red line the projection $\vec{Y}^T a_j$ for the period 11/1970 to 1/1998. The statistical model is tested by comparing the projections $\vec{X}^T b_j$ and $\vec{Y}^T a_j$ outside the fitting period (11/1980 to 1/1998). The skill of the model can be estimated by comparing the black and the red curves. It is concluded that the first four modes have a reasonable high skill. Therefore, they are taken into account for the reconstruction.

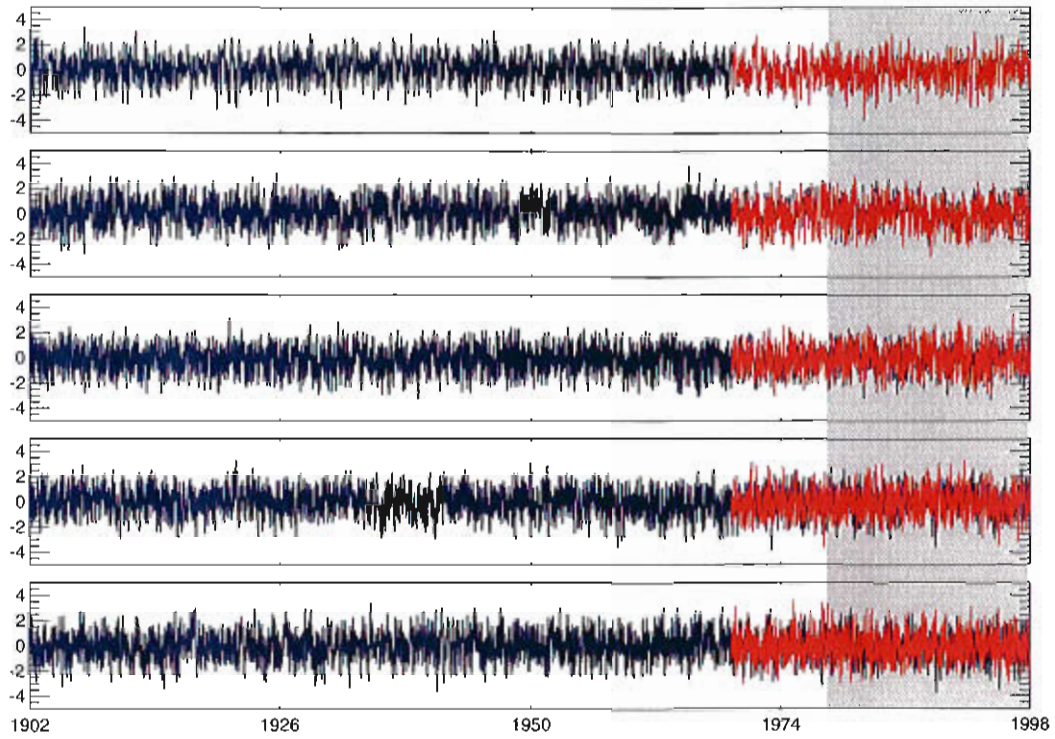

Figure 2: The time series for the first five redundancy modes of the SLP reconstruction in winter. The black line shows the projection $\vec{X}^T b_j$ for 11/1902 to 1/1998. The red line is the projection $\vec{Y}^T a_j$ for the period 11/1970 to 1/1998 where model forcing data exists. The fitting period 11/1980 to 1/1998 is marked by a gray box.

Figure 3 depicts the first redundancy mode. The predictand SLP pattern describes 72% of the variance. The sea level pressure shows an anomaly centered over the northern Baltic Sea with strongest gradients over the Skagerrak-Kattegat. The second redundancy mode (Fig. 4) depicts a dipole with centers over northern Scandinavia and northern Germany. The gridded SLP pattern explains 14% of the variance. The next two modes describe 10% and 3% of the variance, respectively. The redundancy modes of the other seasons are similar to the winter season and will not be described in detail.

Figure 5 shows the explained variances of the statistical model for the fitting and validation periods for all seasons. In all seasons, explained variances between 90 to 100% are achieved over the Baltic Sea in both, the "learning" and the validation period. Lower values are obtained in the south-eastern area of the gridded data, i.e., in regions where no station data exists.

Matthäus and Schinke (1994) argued that the salt water inflows are connected

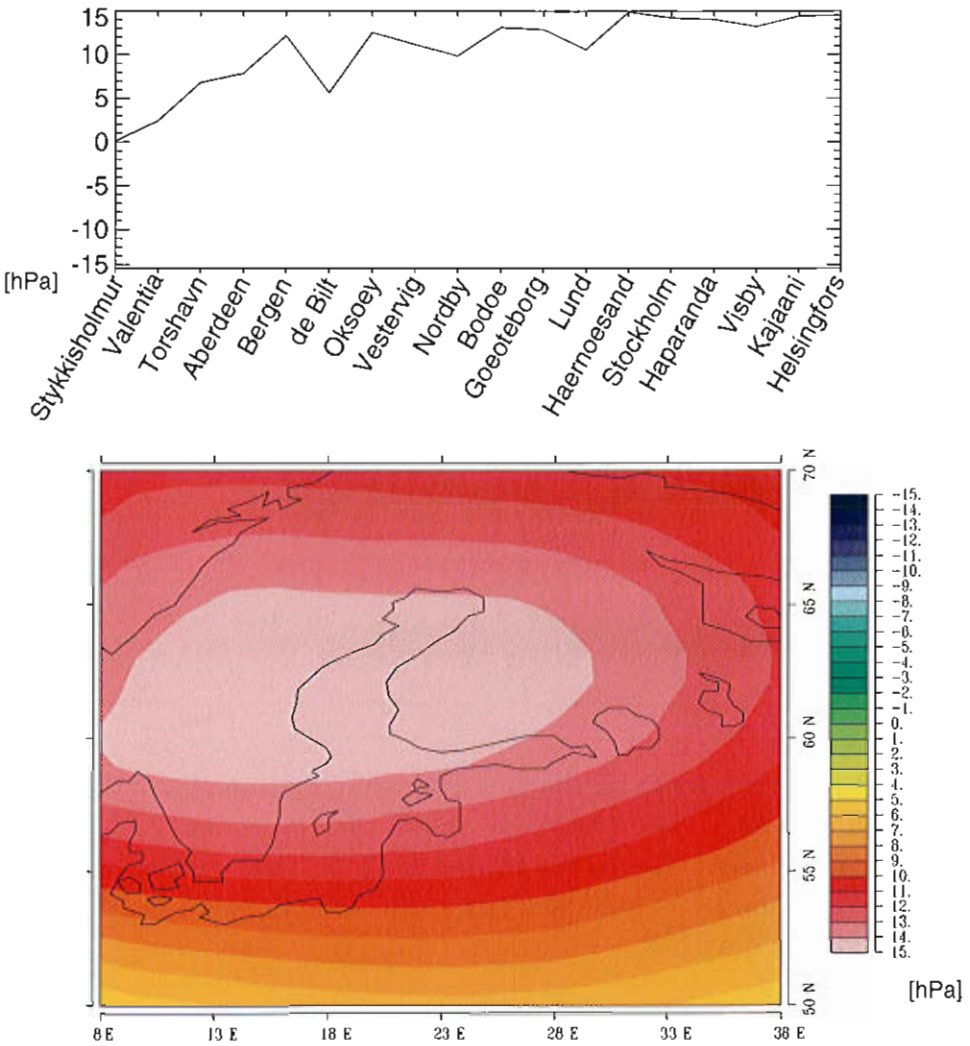

Figure 3: The first redundancy mode. The upper picture shows the station sea level pressure $[hPa]$. The lower panels shows the sea level pressure on the SMHI grid $[hPa]$.

with shifts of the Azores High to north-east two weeks prior to an inflow event. At the same time, the center of lowest pressure moves eastward from the Greenland-Icelandic area to northern Norway. Fig. 6 reveals the cross-spectra of the first and second redundancy mode for winter of the SLP reconstruction. The first and second mode are significantly coherent on time scales of about 15 to 20 days, where the second mode leads the first by a phase of 90°, i.e., the first and second mode describe a propagation of the anomaly described by mode 2 to the anomaly described by mode 1. This does not prove that the reconstruction is able to follow the mechanism described by Matthäus and Schinke (1994), but proves that propagations with consistent time scales are

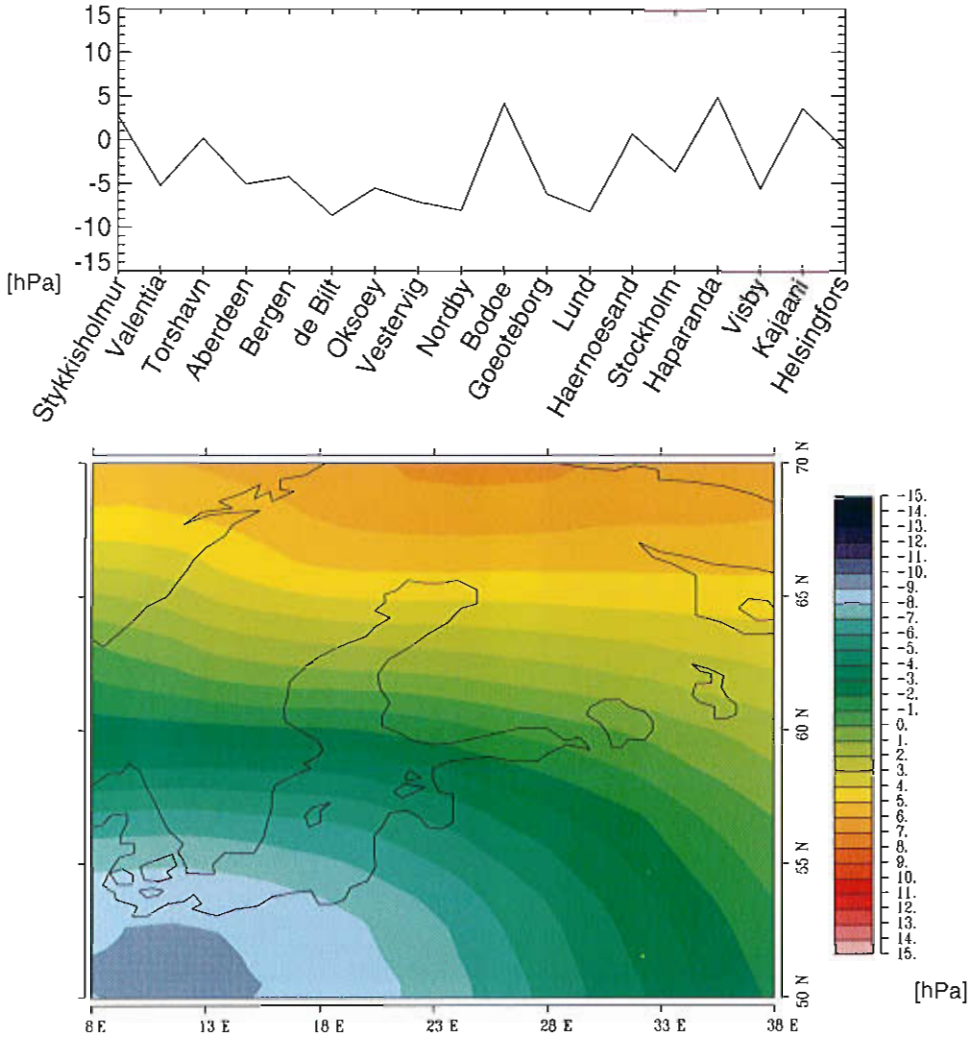

Figure 4: The second redundancy mode. The upper picture shows the station sea level pressure $[hPa]$. The lower panels shows the sea level pressure on the SMHI grid $[hPa]$.

captured by the reconstruction. However, preliminary model results suggest that simulations with the reconstructed surface data are capable to describe salt water events. Also changes of the statistics of such events (higher probability in the 1950s and 1960s compared to the 1980s and 1990s) are reproduced by the model system.

Over the 100 years of reconstructed data no obvious change in the variance of the time series is observed, although it is is documented that the activity of salt water inflows was highest in the 1950s and 1960s and dramatically reduced in the 1980s and 1990s. However, we found a dominant trend in the data. Figure

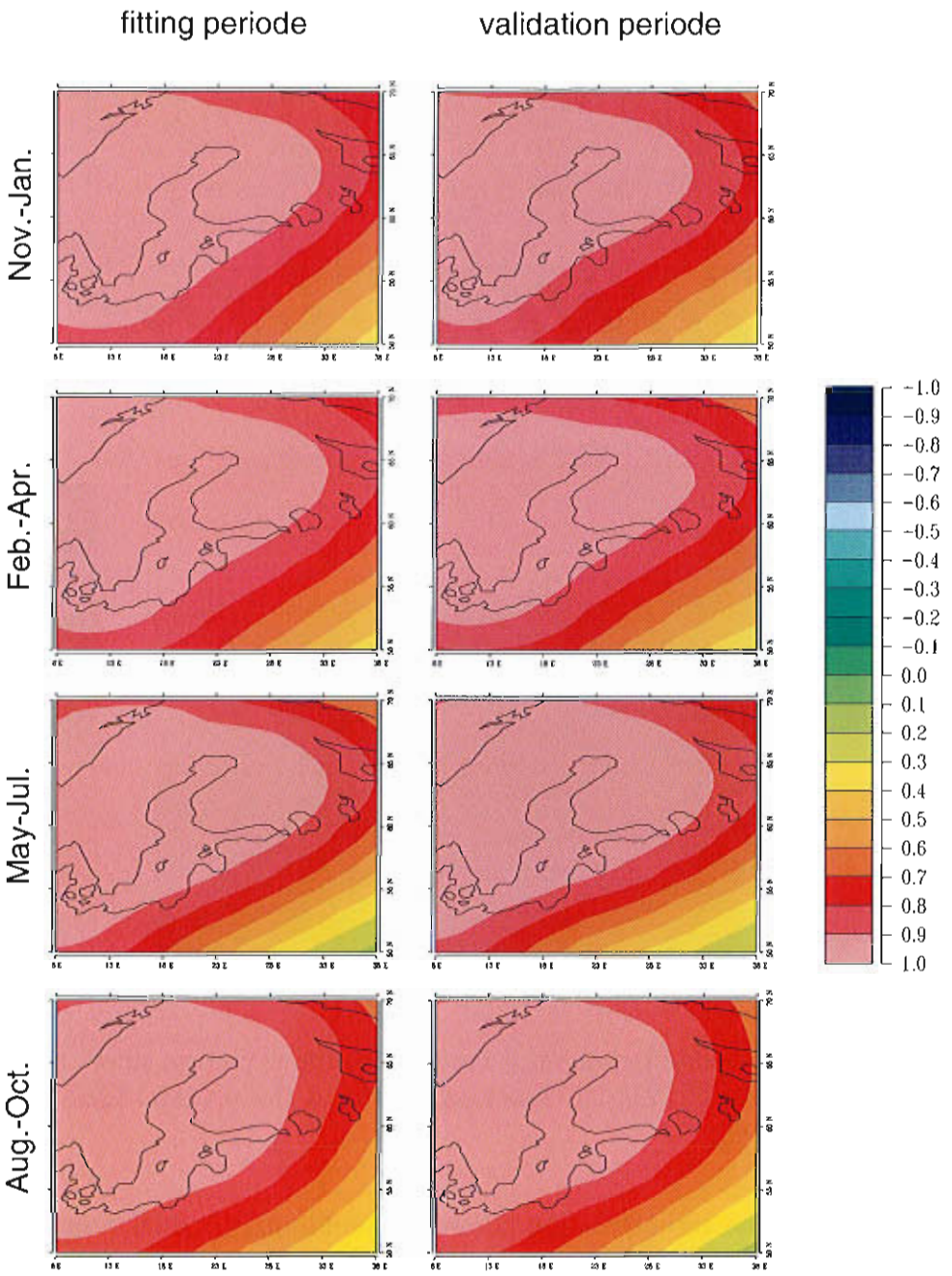

Figure 5: The explained variances of the statistical model for the sea level pressure reconstruction.

7 depicts the mean SLP for the fitting period and the trend for 100 years for all seasons. In winter and spring strong trends are obtained. Compared with the mean state in the 1980s and 1990s the trend in winter reveals a less pronounced zonal geostrophic wind in the mean state in the 1950s and 1960s in winter. In

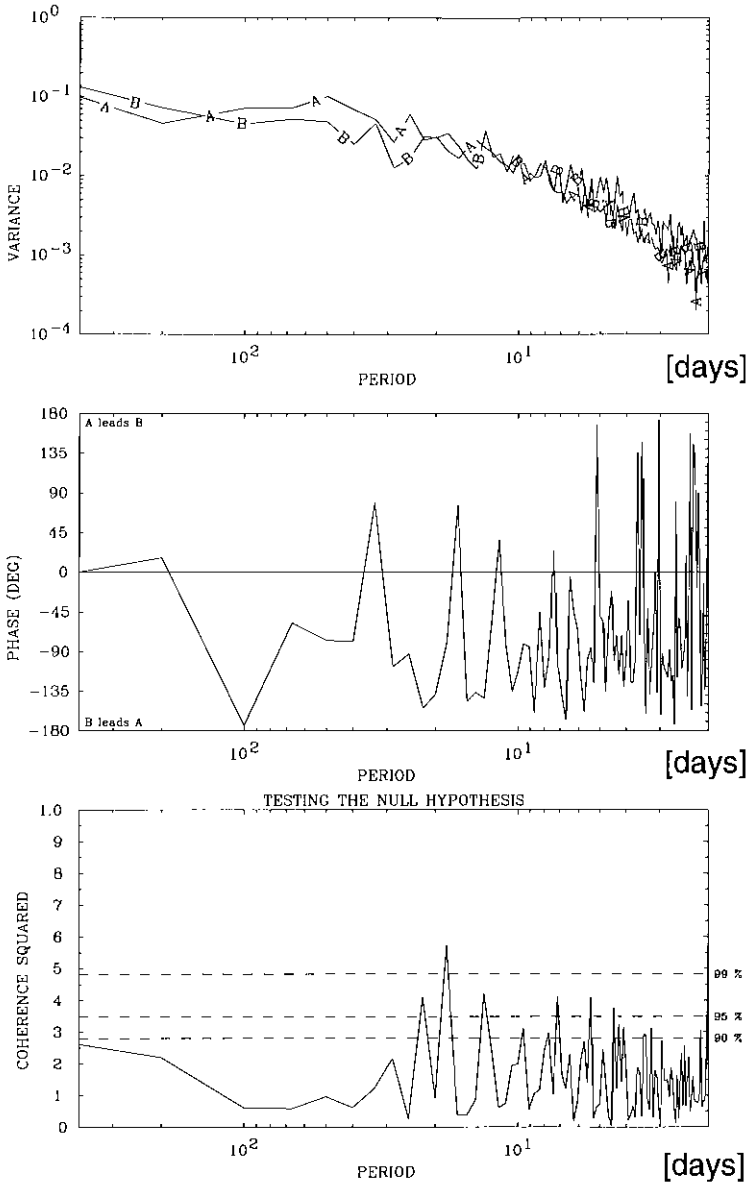

Figure 6: The cross-spectra of the first and second redundancy mode for winter. Top: The spectra of the (A) first and (B) second mode. Middle: The phase relation. Bottom: The squared coherency. A chunk length of 200 days is used to estimate the significance.

spring the zonal geostrophic wind was higher in the 1950s and 1960s than in the 1980s and 1980s which may identify a shift in the seasons during the 100 years.

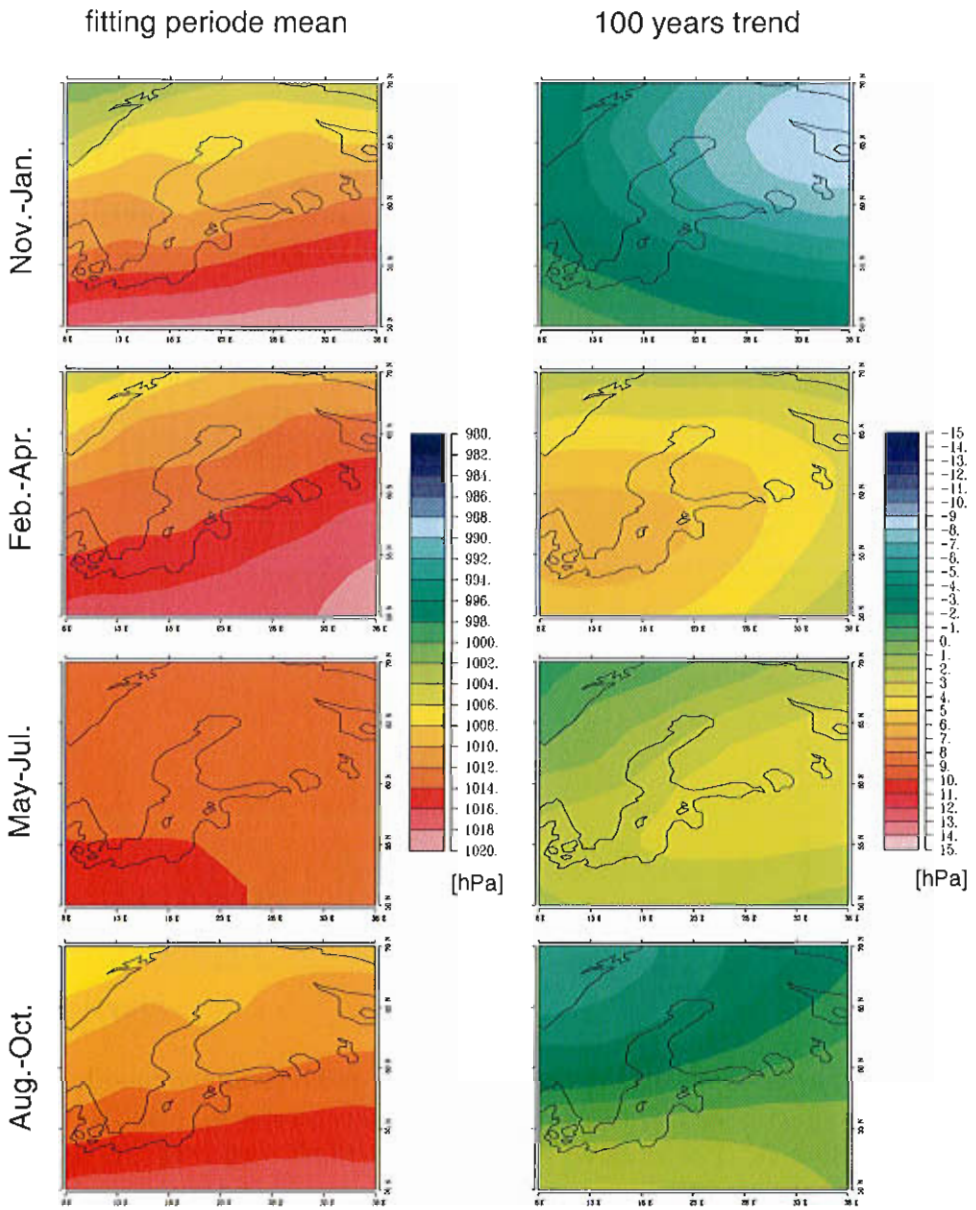

Figure 7: The mean SLP $[hPa]$ in the fitting period and the trend for 100 years of the SLP reconstruction for all seasons.

4.2 2-meter air temperature

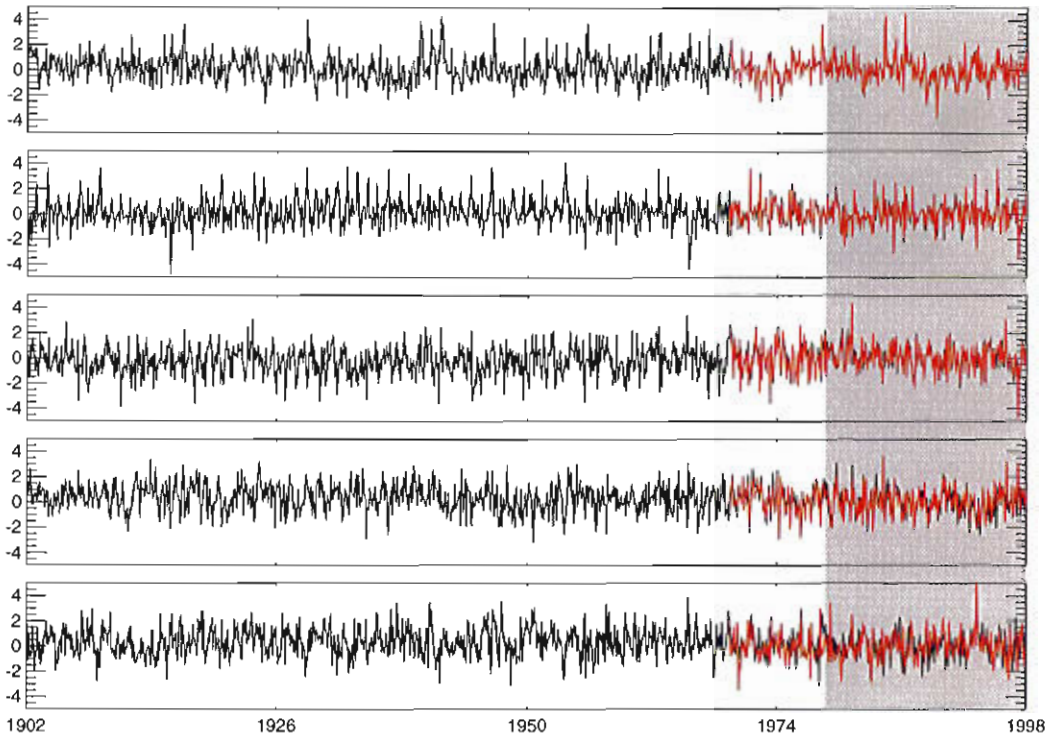

Figure 8: The time series for the first five redundancy modes of the SAT reconstruction. The black line shows the projection $\vec{X}^T b_j$ for 1/1902 to 12/1998. The red line is the projection $\vec{Y}^T a_j$ for the period 1/1970 to 12/1998 where model forcing data exists. The fitting period 1/1980 to 12/1998 is marked by a gray box.

The data from Jones (1994) are used as predictor fields for the SAT. Monthly mean values are employed. The reconstructed time series of the first five leading modes is shown in Figure 8. The correlations in the "learning" period are 0.996, 0.983, 0.960, 0.857, 0.649. The black line shows the projection $\vec{X}^T b_j$ for 1/1902 to 12/1998 and the red line the projection $\vec{Y}^T a_j$ for the period 1/1970 to 12/1998. The statistical model is tested by comparing the projections $\vec{X}^T b_j$ and $\vec{Y}^T a_j$ in the validation period. The skill of all five modes is sufficiently high in the validation period. Therefore, all five modes are taken into account for the reconstruction.

The first two redundancy modes are shown in Figure 9 and 10, respectively. The first five predictand fields describe 73%, 16%, 7%, 2%, and 2% of the variance. For this application the statistical model reduces to a kind of interpolation. The coarse resolution data from Jones (1994) are interpolated with

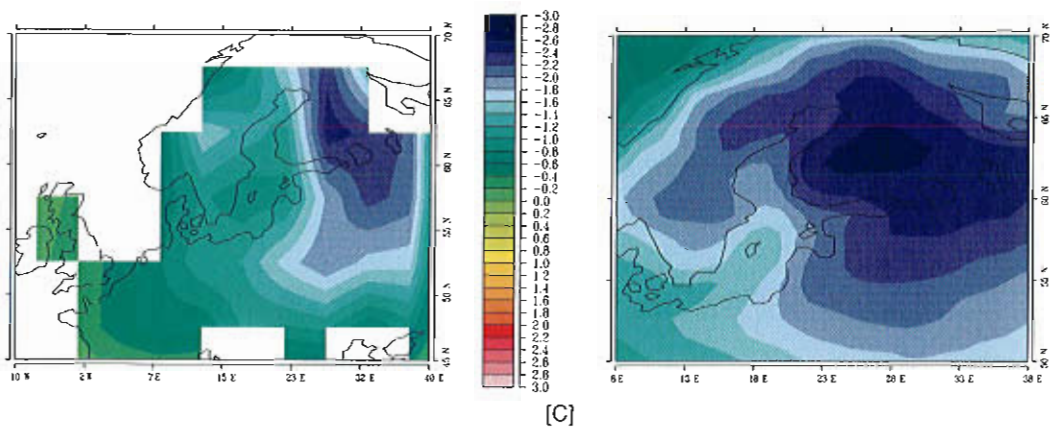

Figure 9: The first redundancy mode of the SAT reconstruction. The left picture shows the SAT data (in $°C$) from Jones (1994). White areas indicate missing values. The predictand field is shown on the right side.

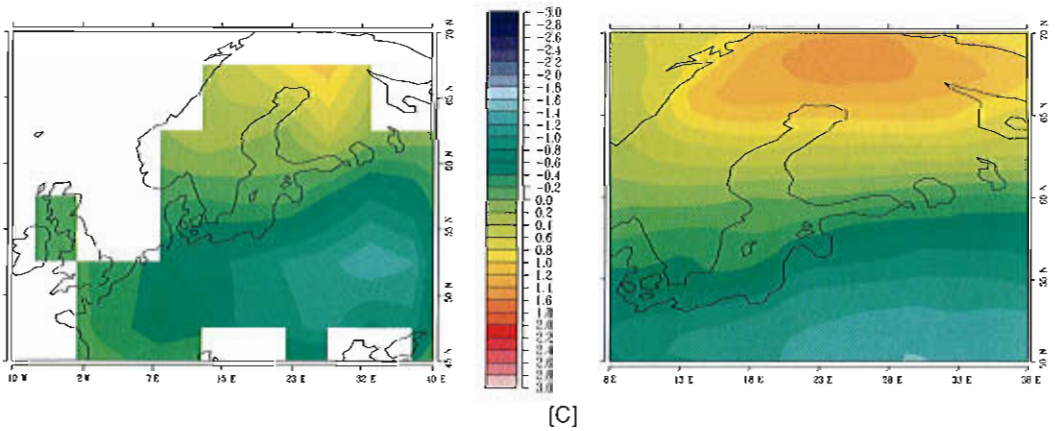

Figure 10: The second redundancy mode of the SAT reconstruction. The left picture shows SAT data $[°C]$ from Jones (1994). White areas indicate missing values. The predictand field is shown on the right side.

the help of the covariance of the finer resolution predictand field. The predictor field of the first mode shows almost no amplitudes over the northern Baltic, whereas the predictand field has a very pronounced gradient over the northern Baltic.

The skill of the reconstruction is higher than 0.9 in huge areas of the predictand field (Fig. 11). Slightly lower skill is achieved in the western Baltic Sea compared to the eastern Baltic Sea.

We found also a pronounced trend for the SAT (Fig.12). The trend is visible

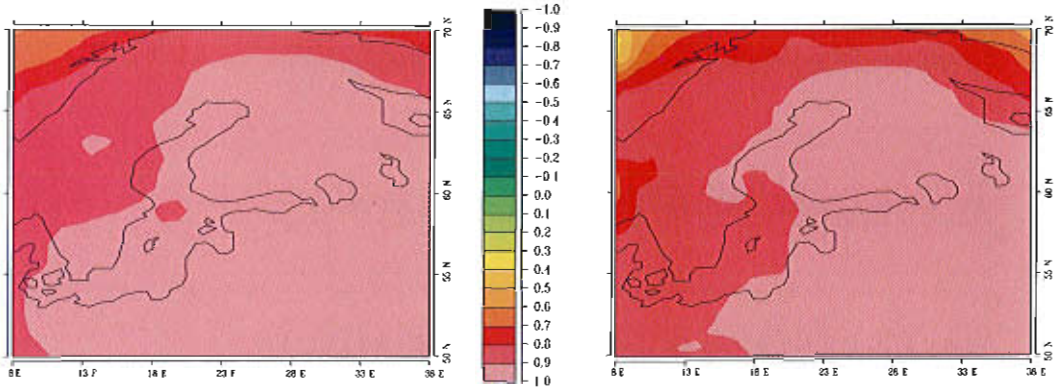

Figure 11: The explained variances for the SAT reconstruction in the fitting period (left) and the validation period (right).

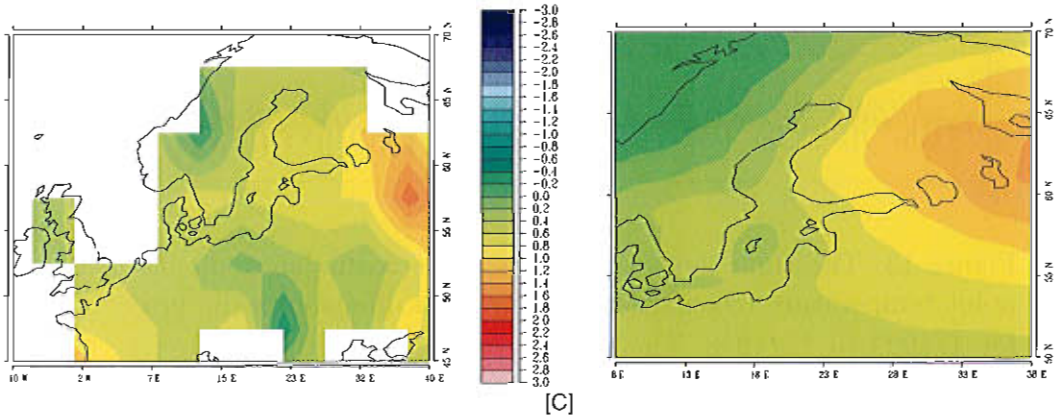

Figure 12: The trend [$^{\circ}C$] for 100 years for the predictor (left) and the predictand (right).

in the predictor and predictand fields but is slightly shifted in the predictand. The trend amounts up to 1.8$^{\circ}C$.

4.3 Relative humidity versus dew-point temperature

For the calculation of the surface fluxes of the Baltic Sea model relative humidity is needed. *A priori* it is not obvious, which of the three predictor fields used is appropriate for the reconstruction. All three predictor field are employed as well as a combination of the three fields: A predictor field is constructed by appending the three predictor fields weighted with their standard deviation. No reasonable high skill is obtained for the relative humidity reconstruction. Therefore, the dew-point temperature is calculated from the relative humidity

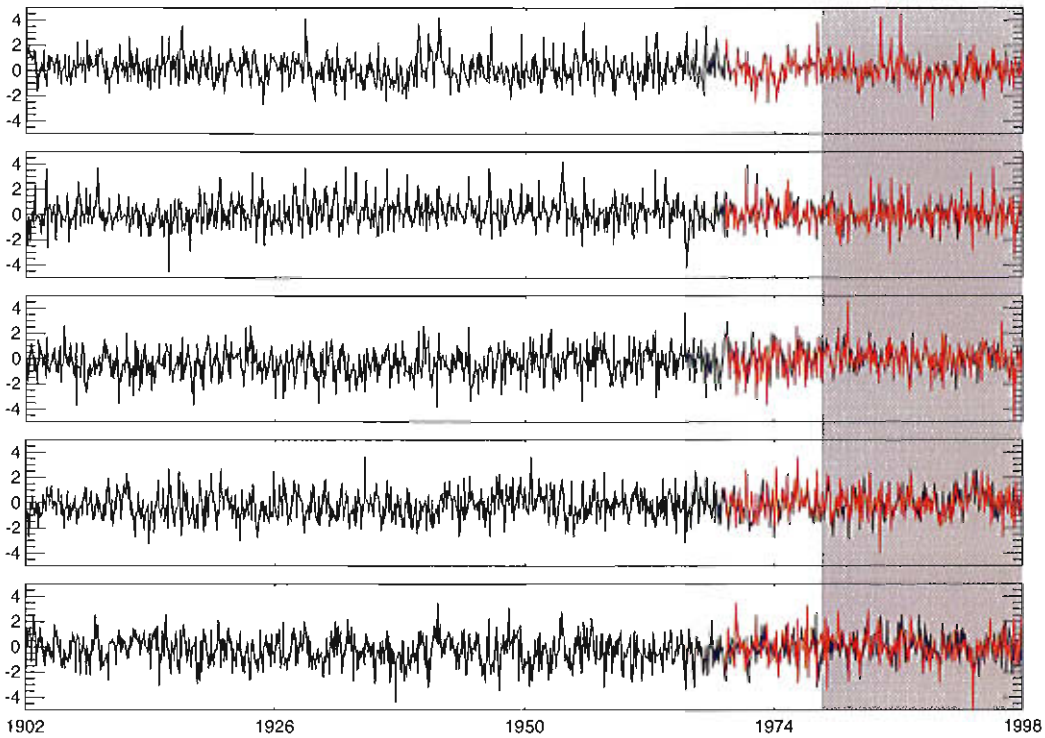

Figure 13: The time series for the first five redundancy modes of the dew-point temperature reconstruction. The black line shows the projection $\vec{X}^T b_j$ for 1/1902 to 12/1998. The red line is the projection $\vec{Y}^T a_j$ for the period 1/1970 to 12/1998 where model forcing data exists. The fitting period 1/1980 to 12/1998 is marked by a gray box.

and employed as the predictand field. The reconstruction with the combination of all three predictor fields yields the highest skill. Using the SAT data from Jones (1994), the skill is only slightly lower. Therefore, the statistical model with the SAT as predictor is presented here and used as model forcing to keep things as simple as possible.

Again, the times series of the first five leading modes are depicted in Figure 13. The correlations in the "learning" period are 0.983, 0.939, 0.922, 0.765, 0.507. All five modes are used for the reconstruction. The first two modes are given in Figures 14 and 15. The patterns are very similar to the corresponding SAT reconstruction patterns. The explained variances are lower than for the SAT reconstruction but still reasonable high (Fig.16).

It should be mentioned here, that the model uses the relative humidity which is calculated from the dew-point temperature and the SAT. Error propagation

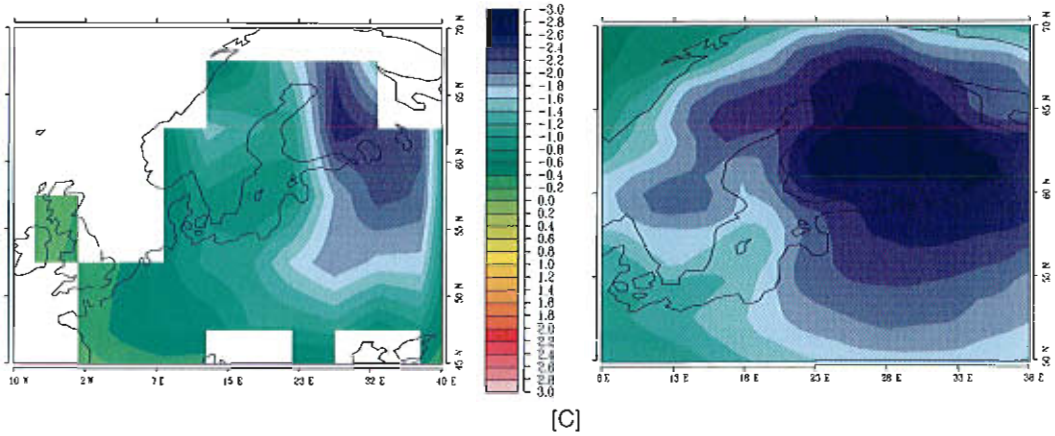

Figure 14: The first redundancy mode of the dew-point temperature reconstruction. The left picture shows the SAT data [^{o}C] from Jones (1994). White areas indicate missing values. The predictand field is shown on the right side.

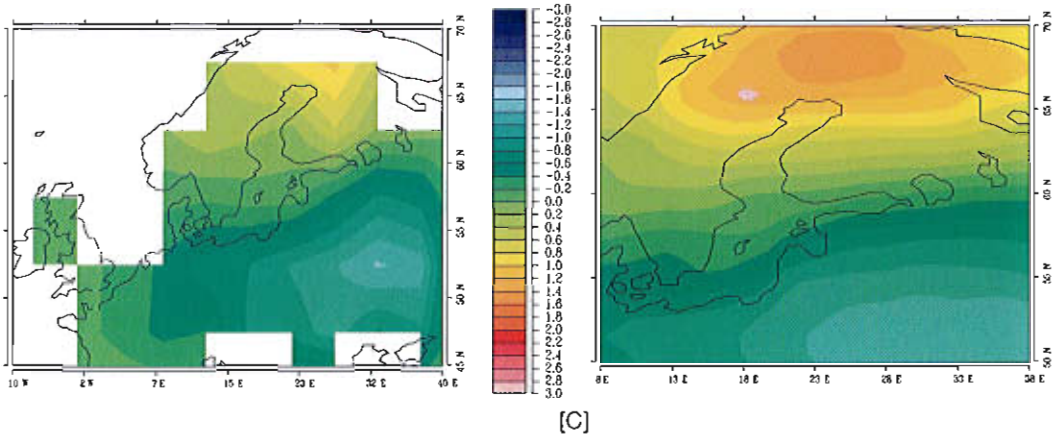

Figure 15: The second redundancy mode of the dew-point temperature reconstruction. The left picture shows the SAT data [^{o}C] from Jones (1994). White areas indicate missing values. The predictand field is shown on the right side.

suggests that the error of the relative humidity might be much higher than the error of the dew-point temperature.

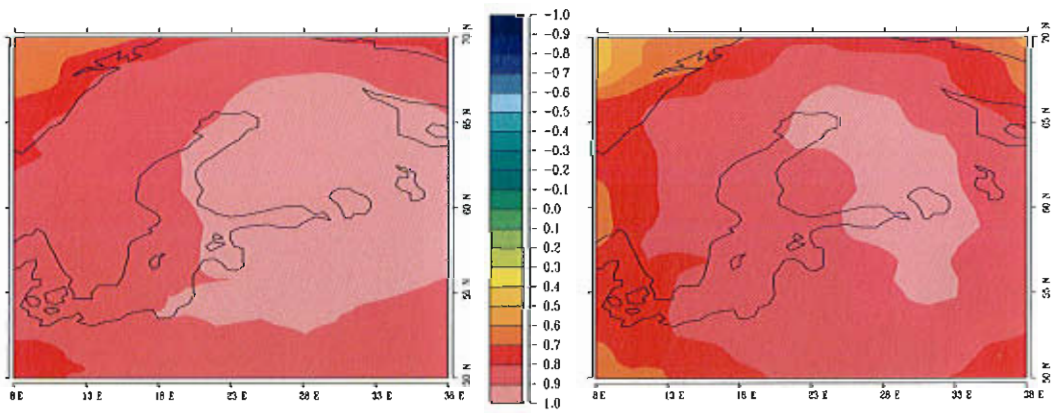

Figure 16: The explained variances for the dew-point temperature reconstruction in the fitting period (left) and the validation period (right).

4.4 Precipitation

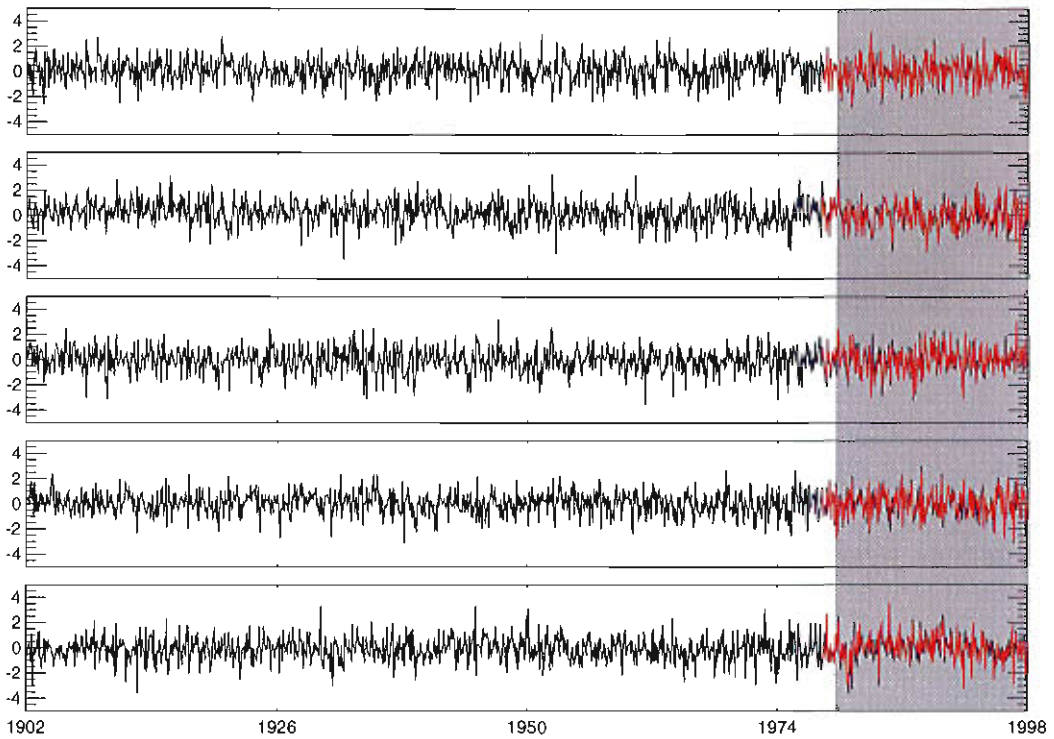

Figure 17: The time series for the first five redundancy modes of the precipitation reconstruction. The black line shows the projection $\vec{X}^T b_j$ for 1/1902 to 12/1998. The red line is the projection $\vec{Y}^T a_j$ for the period 1/1979 to 12/1998 where model forcing data exists. The fitting period 1/1980 to 12/1998 is marked by a gray box.

The data set from Hulme (1992) is used for the reconstruction of precipitation. The predictand data set exists only from 1979 to 1998. Therefore, a validation of the statistical model is not possible. The time series of the first five months are given in Figure 17. Within the "learning" period, the first seven modes have correlations higher than 0.8 and are taken into account. The first two redundancy modes are depicted in Figures 18 and 19. The predictand patterns describe 35%, 23%, 11%, 7%, 5%, 3%, and 2% of the variance. There is a remarkable resemblance between the predictor and predictand field. This may give some confidence to the reconstruction although it could not be tested with independent data. The explained variances of the reconstruction for the "learning" period and for one year of independent data, i.e. 1979, is shown in Figure 20. The explained variances are about 60% in the fitting period. For the one year of independent data a skill of about 70% can be found over almost the whole Baltic with the exception of the northern part.

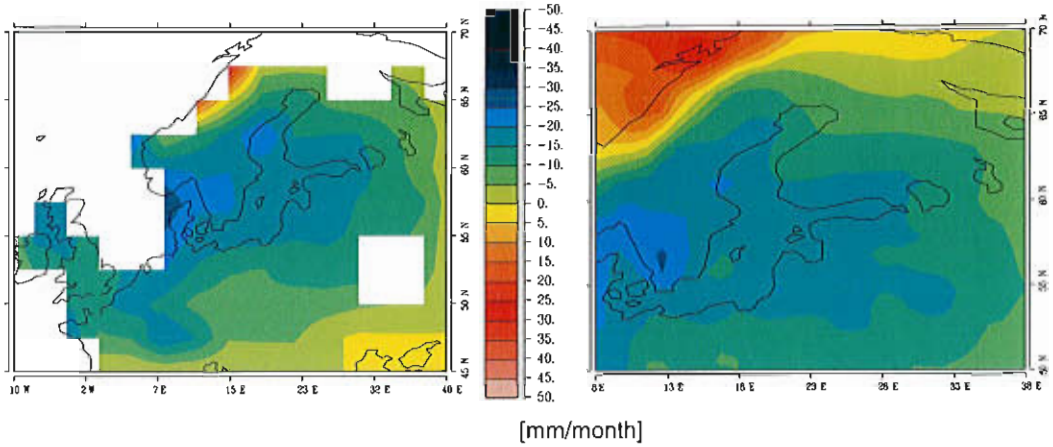

Figure 18: The first redundancy mode of the precipitation reconstruction. The left picture shows data [*mm/month*] from Hulme (1992). White areas indicate missing values. The predictand field is shown on the right side.

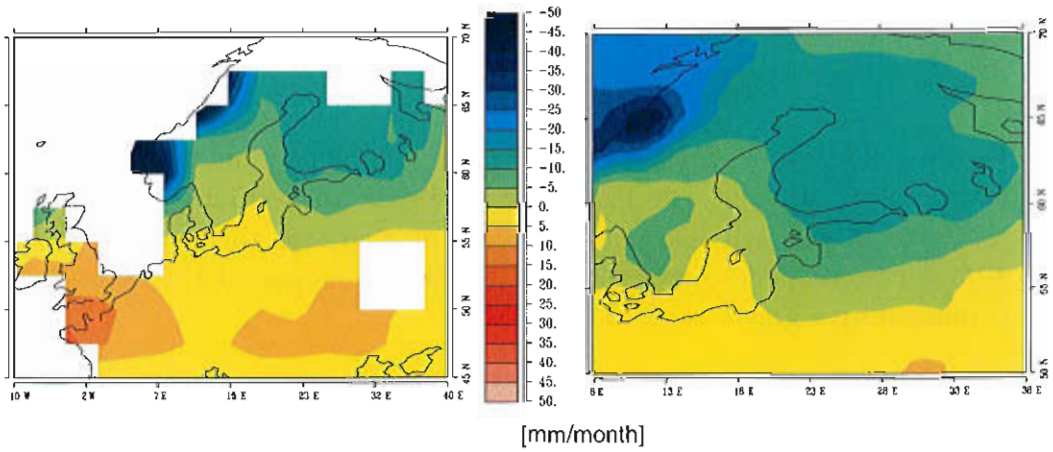

Figure 19: The second redundancy mode of the precipitation reconstruction. The left picture shows data [*mm/month*] from Hulme (1992). White areas indicate missing values. The predictand field is shown on the right side.

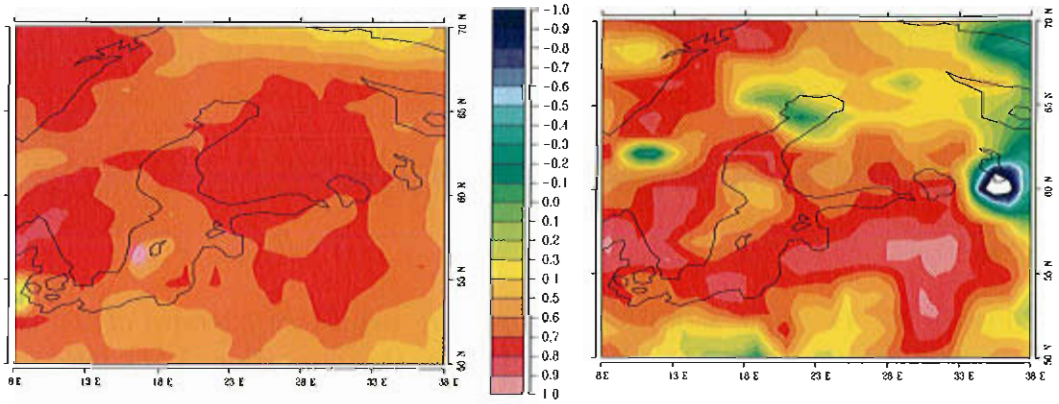

Figure 20: The explained variances for the precipitation reconstruction in the fitting period (left) and for 1979 (right).

4.5 Cloud cover

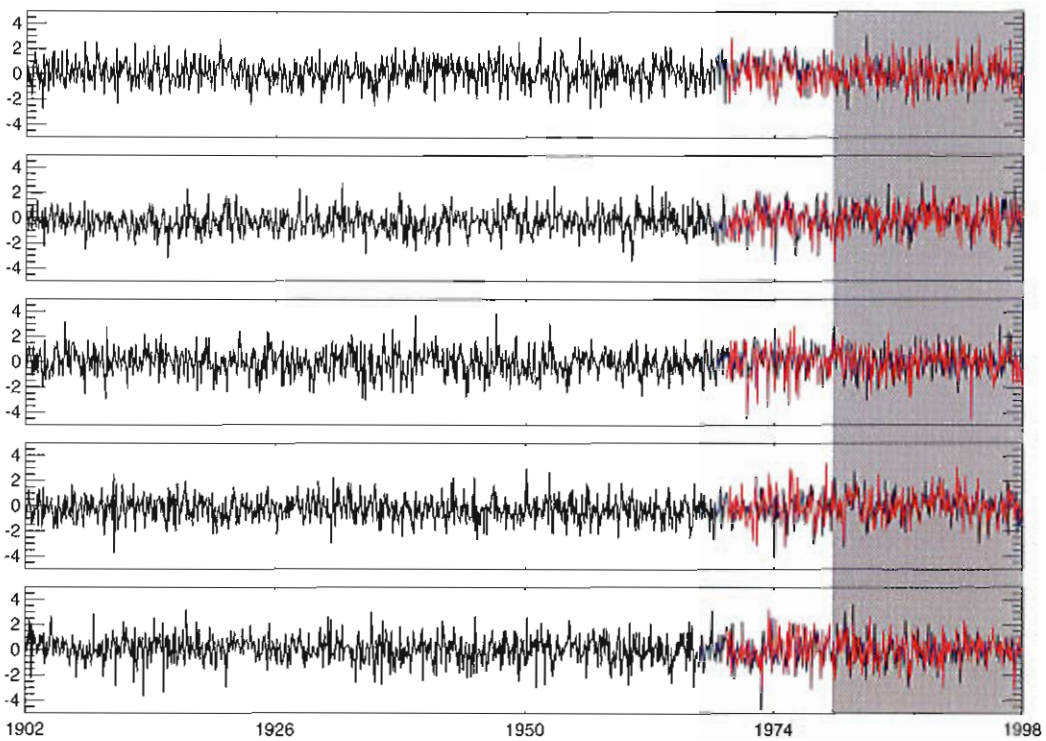

Figure 21: The time series for the first five redundancy modes of the cloud cover reconstruction. The black line shows the projection $\vec{X}^T b_j$ for 1/1902 to 12/1998. The red line is the projection $\vec{Y}^T a_j$ for the period 1/1970 to 12/1998 where model forcing data exists. The fitting period 1/1980 to 12/1998 is marked by a gray box.

The data from Hulme (1992) give the highest skill for the reconstruction of the cloud cover. The time series of the first five leading modes are depicted in Figure 21. The correlations in the "learning" period are smaller than for the other variables but still sufficiently high, i.e. 0.819, 0.766, 0.761, 0.613, 0.466. Seven modes are taken into account for the reconstruction with a correlation greater than 0.5 for the validation period.

The predictand fields explain 44%, 18%, 14%, 6%, 5%, 4%, and 2% of the variance. The first two predictor fields resemble the first two predictor fields of the precipitation reconstruction (Fig. 22 and 23). The explained variances are shown in Figure 24. The skill is rather poor. In Figure 25, the explained variance is shown for 7 month running-mean filtered data for the validation period. The statistical model has a higher skill on longer than monthly time scales.

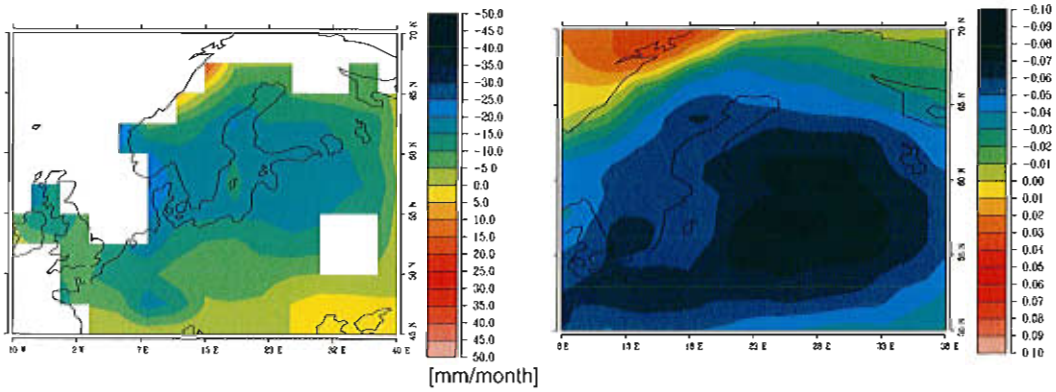

Figure 22: The first redundancy mode of the cloud cover reconstruction. The left picture shows precipitation data [$mm/month$] from Hulme (1992). White areas indicate missing values. The predictand field is shown on the right side.

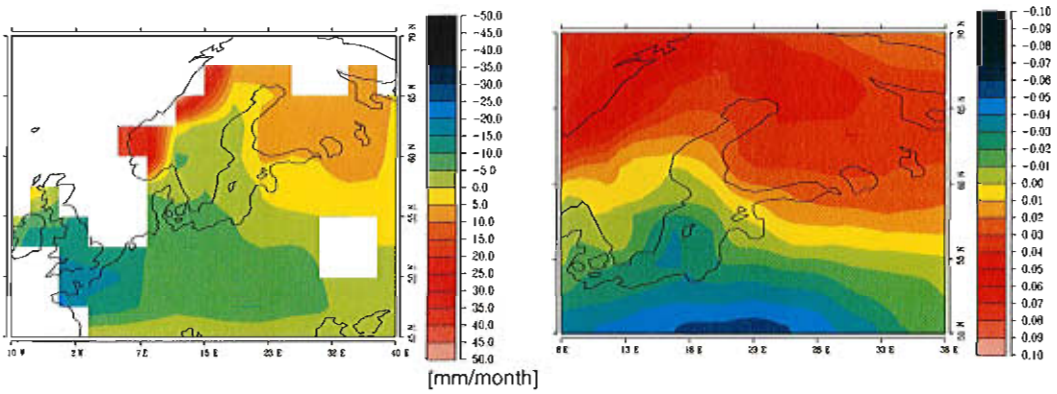

Figure 23: The second redundancy mode of the cloud cover reconstruction. The left picture shows precipitation data [$mm/month$] from Hulme (1992). White areas indicate missing values. The predictand field is shown on the right side.

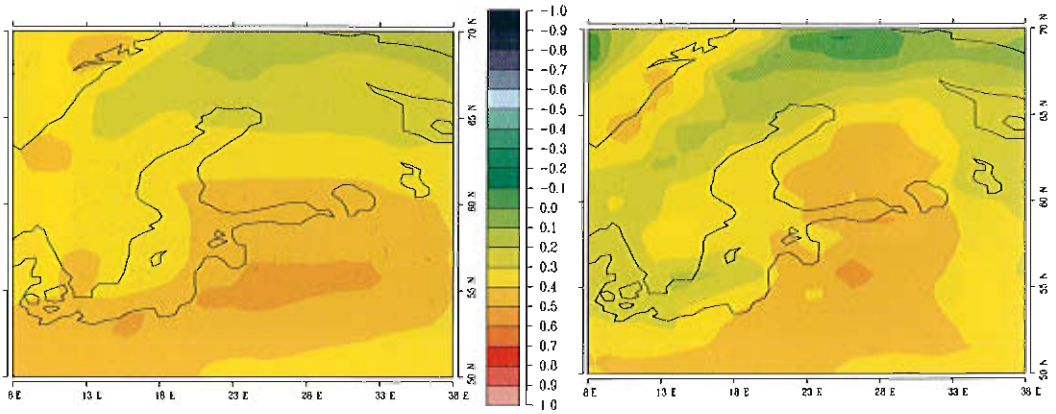

Figure 24: The explained variances for the cloud cover reconstruction in the fitting period (left) and the validation period (right).

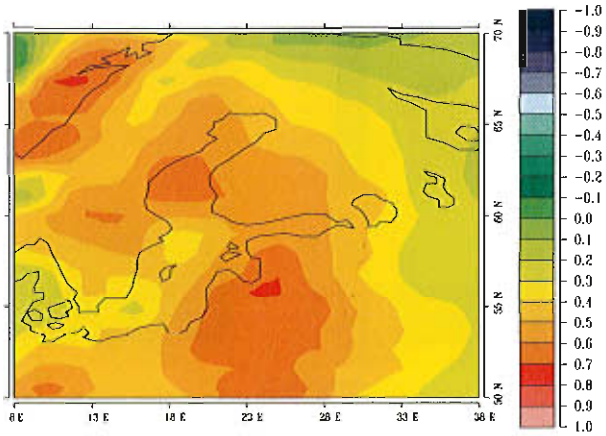

Figure 25: The explained variances for the cloud cover reconstruction in the the validation period for data filtered with a running mean of 7 month.

5 Summary

A technique is presented to allow for the reconstruction of homogeneous atmospheric surface fields for the past 100 years. SLP is reconstructed on the basis of daily data. The skill of the reconstruction is high to very high. Although the degrees of freedom of the reconstructed data is low (four degrees of freedom per season) an analysis reveals propagations in the SLP field. Finally, the model simulations will show if the essential variability is restored by the SLP reconstruction.

The reconstructions of the other surface fields are based on monthly values. SAT and dew-point temperature reconstructions give high skills. As relative humidity is employed by the Baltic Sea model, the skill of the relative humidity may be lower than the skill of the dew-point temperature. Evaporation simulated by the Baltic Sea model will show the quality of the dew-point temperature reconstruction.

The skill of the precipitation reconstruction can not be tested due to the lack of data. However, the similarity of the redundancy patterns gives some confidence to the reconstruction. We found the lowest skill of all variables for cloud cover. The long-term variability has a higher skill than the month-to-month variability.

Acknowledgments

The SWECLIM program and the Rossby Center are funded by the Foundation for Strategic Environmental Research (MISTRA) and by SMHI. Special thanks are given to Hans Alexandersson for providing sea level pressure station data and to Lars Meuller for providing gridded atmospheric surface data for the period 1970-2001.

References

Alexandersson, H., H. Tuomenvirta, T Schmith, and K. Iden, Trends of storms in NW Europe derived from an updated pressure data set, *Clim. Res.*, 14, 71–73, 2000.

Bergström, S., and B. Carlsson, River runoff to the Baltic Sea: 1950-1990, *Ambio*, 23, 280-287, 1994.

Bumke, K., U. Karger, L. Hasse, and K. Niekamp, Evaporation over the Baltic Sea as an example of a semi-enclosed sea, *Contr. Atmos. Phys.*, 71, 249-261, 1998.

Haapala, J., H.E.M. Meier and J. Rinne, Numerical investigations of future ice conditions in the Baltic Sea, *Ambio*, 30, 237-244, 2001.

Hilmer, M., and T. Jung, Evidence for a recent change in the link between the North Atlantic Oscillation and Arctic sea ice export, *Geophys. Res. Lett.*, 27, 989-992, 2000.

Hulme, M., A 1951-80 global land precipitation climatology for the evaluation of General Circulation Models, *Clim. Dyn.*, 7, 57–72, 1992.

Hulme, M., Validation of large-scale precipitation fields in General Circulation Models, pp.387–406, in: Global precipitations and climate change, (eds.) Desbois, M. and Desalmand, F., NATO ASI Series, Springer-Verlag, Berlin, 466pp, 1994.

Hulme, M., Osborn, T.J. and T.C. Johns, Precipitation sensitivity to global warming: Comparison of observations with HadCM2 simulations, *Geophys. Res. Let.*, 25, 3379–3382, 1998.

Jones, P.D., Hemispheric surface air temperature variations: a reanalysis and an update to 1993, *J. Climate,* 7, 1794–1802, 1994.

Knudsen, M., The hydrographic conditions in the Danish waters inside Skagen in 1894-98 (in Danish), *Komm For Vidensk Unders I de danske farvande*, 2, 2, 1899.

Knudsen, M., A hydrographical theorem (in German), *Ann. Hydr.*, 28, 316-320, 1900.

Lass, H.U., and W. Matthäus, On temporal wind variations forcing salt water inflows into the Baltic Sea, *Tellus*, 48A, 663-671, 1996.

Matthäus, W., and H. Franck, Characteristics of major Baltic inflows - a statistical analysis, *Cont. Shelf Res.*, 12, 1375-1400, 1992.

Matthäus, W., and H.U. Lass, The recent salt inflow into the Baltic Sea, *J. Phys. Oceanogr.*, 25, 280-286, 1995.

Matthäus, W., and H. Schinke, Mean atmospheric circulation patterns associated with major Baltic inflows, *Deutsch. Hydr. Zeitschr.*, 46, 321-339, 1994.

Matthäus, W., and H. Schinke, The influence of river runoff on deep water conditions of the Baltic Sea, *Hydrobiologia*, 393, 1-10, 1999.

Meier, H.E.M., First results of multi-year simulations using a 3D Baltic Sea model, Reports Oceanography No.27, SMHI, Norrköping, Sweden, 48 pp, 1999.

Meier, H.E.M., R. Döscher, A.C. Coward, J. Nycander and K. Döös, RCO - Rossby Centre regional Ocean climate model: model description (version 1.0) and first results from the hindcast period 1992/93, Reports Oceanography No.26, SMHI, Norrköping, Sweden, 102 pp, 1999.

Meier, H.E.M., The use of the $k-\epsilon$ turbulence model within the Rossby Centre regional ocean climate model: parameterization development and results, Reports Oceanography No. 28, SMHI, Norrköping, Sweden, 81 pp, 2000.

Meier, H.E.M., The first Rossby Centre regional climate scenario for the Baltic Sea using a 3D coupled ice-ocean model, Reports Meteorology and Climatology No.95, SMHI, Norrköping, Sweden, 63 pp, 2001a.

Meier, H.E.M., On the parameterization of mixing in 3D Baltic Sea models, *J. Geophys. Res.*, 106, 30997-31016, 2001b.

Meier, H.E.M., Regional ocean climate simulations with a 3D ice-ocean model for the Baltic Sea. Part 1: Model experiments and results for temperature and salinity, *Clim. Dyn.*, 18, accepted, 2002a.

Meier, H.E.M., Regional ocean climate simulations with a 3D ice-ocean model for the Baltic Sea. Part 2: Results for sea ice, *Clim. Dyn.*, 18, accepted, 2002b.

Meier, H.E.M., and T. Faxén, 2002: Performance analysis of a multiprocessor

coupled ice-ocean model for the Baltic Sea, *J. Atmos. Oceanic Technol.*, 19, 114-124, 2002.

Meier, H.E.M., R. Döscher and T. Faxén, A multiprocessor coupled ice-ocean model for the Baltic Sea: application to salt inflow, *J. Geophys. Res.*, submitted, 2002.

Omstedt, A., L. Nyberg, and L. Meuller, Interannual, seasonal and regional variations of precipitation and evaporation over the Baltic Sea, *Ambio*, 26, 644-662, 1997.

Schinke, H., and W. Matthäus, On the causes of major Baltic inflows - an analysis of long time series, *Cont. Shelf Res.*, 18, 67-97, 1998.

Seifert, T., and B. Kayser, A high resolution spherical grid topography of the Baltic Sea, *Meereswiss. Ber., Warnemünde*, 9, 73-88, 1995.

Sjöberg, B. (ed.), Sea and Coast, The National Atlas of Sweden, Almqvist and Wiksell International, Stockholm, 128 pp, 1992.

Tyler, D.E., On the optimality of the simultaneous redundancy transformations, *Psychometrica,* 47, 77-86, 1982.

von Storch, H., and F. Zwiers, Statistical analysis in climate research, Cambridge University Press, UK, 1998.

Welander, P., Two-layer exchange in an estuary basin, with special reference to the Baltic Sea, *J. Phys. Oceanogr.*, 4, 542-556, 1974.

SMHIs publications

SMHI publishes six report series. Three of these, the R-series, are intended for international readers and are in most cases written in English. For the others the Swedish language is used.

Names of the Series	**Published since**
RMK (Report Meteorology and Climatology)	1974
RH (Report Hydrology)	1990
RO (Report Oceanography)	1986
METEOROLOGI	1985
HYDROLOGI	1985
OCEANOGRAFI	1985

Earlier issues published in serie RMK

1 Thompson, T., Udin, I., and Omstedt, A. (1974)
Sea surface temperatures in waters surrounding Sweden.

2 Bodin, S. (1974)
Development on an unsteady atmospheric boundary layer model.

3 Moen, L. (1975)
A multi-level quasi-geostrophic model for short range weather predictions.

4 Holmström, I. (1976)
Optimization of atmospheric models.

5 Collins, W.G. (1976)
A parameterization model for calculation of vertical fluxes of momentum due to terrain induced gravity waves.

6 Nyberg, A. (1976)
On transport of sulphur over the North Atlantic.

7 Lundqvist, J.-E., and Udin, I. (1977)
Ice accretion on ships with special emphasis on Baltic conditions.

8 Eriksson, B. (1977)
Den dagliga och årliga variationen av temperatur, fuktighet och vindhastighet vid några orter i Sverige.

9 Holmström, I., and Stokes, J. (1978)
Statistical forecasting of sea level changes in the Baltic.

10 Omstedt, A., and Sahlberg, J. (1978)
Some results from a joint Swedish-Finnish sea ice experiment, March, 1977.

11 Haag, T. (1978)
Byggnadsindustrins väderberoende, seminarieuppsats i företagsekonomi, B-nivå.

12 Eriksson, B. (1978)
Vegetationsperioden i Sverige beräknad från temperaturobservationer.

13 Bodin, S. (1979)
En numerisk prognosmodell för det atmosfäriska gränsskiktet, grundad på den turbulenta energiekvationen.

14 Eriksson, B. (1979)
Temperaturfluktuationer under senaste 100 åren.

15 Udin, I., och Mattisson, I. (1979)
Havsis- och snöinformation ur datorbearbetade satellitdata - en modellstudie.

16 Eriksson, B. (1979)
Statistisk analys av nederbördsdata. Del I. Arealnederbörd.

17 Eriksson, B. (1980)
Statistisk analys av nederbördsdata. Del II. Frekvensanalys av månadsnederbörd.

18 Eriksson, B. (1980)
Årsmedelvärden (1931-60) av nederbörd, avdunstning och avrinning.

19 Omstedt, A. (1980)
A sensitivity analysis of steady, free floating ice.

20 Persson, C., och Omstedt, G. (1980)
En modell för beräkning av luftföroreningars spridning och deposition på mesoskala.

21 Jansson, D. (1980)
Studier av temperaturinversioner och vertikal vindskjuvning vid Sundsvall-Härnösands flygplats.

22 Sahlberg, J., and Törnevik, H. (1980)
A study of large scale cooling in the Bay of Bothnia.

23 Ericson, K., and Hårsmar, P.-O. (1980)
Boundary layer measurements at Klock-rike. Oct. 1977.

24 Bringfelt, B. (1980)
A comparison of forest evapotranspiration determined by some independent methods.

25 Bodin, S., and Fredriksson, U. (1980)
Uncertainty in wind forecasting for wind power networks.

26 Eriksson, B. (1980)
Graddagsstatistik för Sverige.

27 Eriksson, B.(1981)
Statistisk analys av nederbördsdata. Del III. 200-åriga nederbördsserier.

28 Eriksson, B. (1981)
Den "potentiella" evapotranspirationen i Sverige.

29 Pershagen, H. (1981)
Maximisnödjup i Sverige (perioden 1905-70).

30 Lönnqvist, O. (1981)
Nederbördsstatistik med praktiska tillämpningar.
(Precipitation statistics with practical applications.)

31 Melgarejo, J.W. (1981)
Similarity theory and resistance laws for the atmospheric boundary layer.

32 Liljas, E. (1981)
Analys av moln och nederbörd genom automatisk klassning av AVHRR-data.

33 Ericson, K. (1982)
Atmospheric boundary layer field experiment in Sweden 1980, GOTEX II, part I.

34 Schoeffler, P. (1982)
Dissipation, dispersion and stability of numerical schemes for advection and diffusion.

35 Undén, P. (1982)
The Swedish Limited Area Model. Part A. Formulation.

36 Bringfelt, B. (1982)
A forest evapotranspiration model using synoptic data.

37 Omstedt, G. (1982)
Spridning av luftförorening från skorsten i konvektiva gränsskikt.

38 Törnevik, H. (1982)
An aerobiological model for operational forecasts of pollen concentration in the air.

39 Eriksson, B. (1982)
Data rörande Sveriges temperaturklimat.

40 Omstedt, G. (1984)
An operational air pollution model using routine meteorological data.

41 Persson, C., and Funkquist, L. (1984)
Local scale plume model for nitrogen oxides. Model description.

42 Gollvik, S. (1984)
Estimation of orographic precipitation by dynamical interpretation of synoptic model data.

43 Lönnqvist, O. (1984)
Congression - A fast regression technique with a great number of functions of all predictors.

44 Laurin, S. (1984)
Population exposure to SO and NO_x from different sources in Stockholm.

45 Svensson, J. (1985)
Remote sensing of atmospheric tempera-ture profiles by TIROS Operational Vertical Sounder.

46 Eriksson, B. (1986)
Nederbörds- och humiditetsklimat i Sverige under vegetationsperioden.

47 Taesler, R. (1986)
Köldperioden av olika längd och förekomst.

48 Wu Zengmao (1986)
Numerical study of lake-land breeze over Lake Vättern, Sweden.

49 Wu Zengmao (1986)
Numerical analysis of initialization procedure in a two-dimensional lake breeze model.

50 Persson, C. (1986)
Local scale plume model for nitrogen oxides. Verification.

51 Melgarejo, J.W. (1986)
An analytical model of the boundary layer above sloping terrain with an application to observations in Antarctica.

52 Bringfelt, B. (1986)
Test of a forest evapotranspiration model.

53 Josefsson, W. (1986)
Solar ultraviolet radiation in Sweden.

54 Dahlström, B. (1986)
Determination of areal precipitation for the Baltic Sea.

55 Persson, C. (SMHI), Rodhe, H. (MISU), De Geer, L.-E. (FOA) (1986)
The Chernobyl accident - A meteorological analysis of how radionucleides reached Sweden.

56 Persson, C., Robertson, L. (SMHI), Grennfelt, P., Kindbom, K., Lövblad, G., och Svanberg, P.-A. (IVL) (1987)
Luftföroreningsepisoden över södra Sverige 2 - 4 februari 1987.

57 Omstedt, G. (1988)
An operational air pollution model.

58 Alexandersson, H., Eriksson, B. (1989)
Climate fluctuations in Sweden 1860 - 1987.

59 Eriksson, B. (1989)
Snödjupsförhållanden i Sverige - Säsongerna 1950/51 - 1979/80.

60 Omstedt, G., Szegö, J. (1990)
Människors exponering för luftföroreningar.

61 Mueller, L., Robertson, L., Andersson, E., Gustafsson, N. (1990)
Meso-γ scale objective analysis of near surface temperature, humidity and wind, and its application in air pollution modelling.

62 Andersson, T., Mattisson, I. (1991)
A field test of thermometer screens.

63 Alexandersson, H., Gollvik, S., Meuller, L. (1991)
An energy balance model for prediction of surface temperatures.

64 Alexandersson, H., Dahlström, B. (1992)
Future climate in the Nordic region - survey and synthesis for the next century.

65 Persson, C., Langner, J., Robertson, L. (1994)
Regional spridningsmodell för Göteborgs och Bohus, Hallands och Älvsborgs län. (A mesoscale air pollution dispersion model for the Swedish west-coast region. In Swedish with captions also in English.)

66 Karlsson, K.-G. (1994)
Satellite-estimated cloudiness from NOAA AVHRR data in the Nordic area during 1993.

67 Karlsson, K-G. (1996)
Cloud classifications with the SCANDIA model.

68 Persson, C., Ullerstig, A. (1996)
Model calculations of dispersion of lindane over Europe. Pilot study with comparisons to measurements around the Baltic Sea and the Kattegat.

69 Langner, J., Persson, C., Robertson, L., and Ullerstig, A. (1996)
Air pollution Assessment Study Using the MATCH Modelling System. Application to sulfur and nitrogen compounds over Sweden 1994.

70 Robertson, L., Langner, J., Engardt, M. (1996)
MATCH - Meso-scale Atmosperic Transport and Chemistry modelling system.

71 Josefsson, W. (1996)
Five years of solar UV-radiation monitoring in Sweden.

72 Persson, C., Ullerstig, A., Robertson, L., Kindbom, K., Sjöberg, K. (1996)
The Swedish Precipitation Chemistry Network. Studies in network design using the MATCH modelling system and statistical methods.

73 Robertson, L. (1996)
Modelling of anthropogenic sulfur deposition to the African and South American continents.

74 Josefsson, W. (1996)
Solar UV-radiation monitoring 1996.

75 Häggmark, L., Ivarsson, K.-I. (SMHI), Olofsson, P.-O. (Militära vädertjänsten). (1997)
MESAN - Mesoskalig analys.

76 Bringfelt, B, Backström, H, Kindell, S, Omstedt, G, Persson, C, Ullerstig, A. (1997)
Calculations of PM-10 concentrations in Swedish cities- Modelling of inhalable particles

77 Gollvik, S. (1997)
The Teleflood project, estimation of precipitation over drainage basins.

78 Persson, C., Ullerstig, A. (1997)
Regional luftmiljöanalys för Västmanlands län baserad på MATCH modell-beräkningar och mätdata - Analys av 1994 års data

79 Josefsson, W., Karlsson, J.-E. (1997)
Measurements of total ozone 1994-1996.

80 Rummukainen, M. (1997)
Methods for statistical downscaling of GCM simulations.

81 Persson, T. (1997)
Solar irradiance modelling using satellite retrieved cloudiness - A pilot study

82 Langner, J., Bergström, R. (SMHI) and Pleijel, K. (IVL) (1998)
European scale modelling of sulfur, oxidized nitrogen and photochemical oxidants. Model development and evaluation for the 1994 growing season.

83 Rummukainen, M., Räisänen, J., Ullerstig, A., Bringfelt, B., Hansson, U., Graham, P., Willén, U. (1998)
RCA - Rossby Centre regional Atmospheric climate model: model description and results from the first multi-year simulation.

84 Räisänen, J., Döscher, R. (1998)
Simulation of present-day climate in Northen Europé in the HadCM2 OAGCM.

85 Räisänen, J., Rummukainen, M., Ullerstig, A., Bringfelt, B., Ulf Hansson, U., Willén, U. (1999)
The First Rossby Centre Regional Climate Scenario - Dynamical Downscaling of CO_2-induced Climate Change in the HadCM2 GCM.

86 Rummukainen, Markku. (1999)
On the Climate Change debate

87 Räisänen, Jouni (2000)
CO_2-induced climate change in northern Europé: comparison of 12 CMIP2 experiments.

88 Engardt, Magnuz (2000)
Sulphur simulations for East Asia using the MATCH model with meteorological data from ECMWF.

89 Persson, Thomas (2000)
Measurements of Solar Radiation in Sweden 1983-1998

90 Daniel B. Michelson, Tage Andersson
Swedish Meteorological and Hydrological Institute (2000)
Jarmo Koistinen, Finnish Meteorological Institute
Christopher G. Collier, Telford Institute of Environmental Systems, University of Salford
Johann Riedl, German Weather Service
Jan Szturc, Instiute of Meteorology and Water Management
Uta Gjertsen, The Norwegian Meteorological Institute
Aage Nielsen, Danish Meteorological Institute
Søren Overgaard, Danish Meteorological Institute
BALTEX Radar Data Centre Products and their Methodologies

91 Josefsson, Weine (2000)
Measurements of total ozone 1997 – 1999

92 Andersson, Tage (2000)
Boundary clear air echos in southern Sweden

93 Andersson, Tage (2000)
Using the Sun to check some weather radar parameters

94 Rummukainen, M.,S. Bergström, E. Källén, L. Moen, J. Rodhe, M. Tjernström (2000)
SWECLIM – The First Three Years

95 Meier, H. E Markus (2001)
The first Rossby Centre regional climate scenario for the Baltic Sea using a 3D coupled ice-ocean model

96 Landelius, Tomas, Weine Josefsson, Thomas Persson (2001)
A system for modelling solar radiation parameters with mesoscale spatial resolution

97 Karlsson, Karl-Göran (2001)
A NOAA AVHRR cloud climatology over Scandinavia covering the period 1991-2000

98 Bringfelt, B., Räisänen, J., Gollvik, S., Lindström, G., Graham, P., Ullerstig, A., (2001)
The land surface treatment for the Rossby Centre Regional Atmospheric Climate Model - version 2 (RCA2)

SMHI
Swedish Meteorological and Hydrological Institute
SE 601 76 Norrköping, Sweden.
Tel +46 11-495 80 00. Fax +46 11-495 80 01

ISSN 0347-2116